Research Square

Preprints are preliminary reports that have not undergone peer review.
They should not be considered conclusive, used to inform clinical practice,
or referenced by the media as validated information.

ATR-FTIR Spectroscopy Combined with Chemometric Methods for the Classification of Polyethylene Residues Containing Different Contaminants

Daniel José da Silva (dankuruta@hotmail.com)
USP: Universidade de Sao Paulo
Hélio Wiebeck
USP: Universidade de Sao Paulo

Research Article

Keywords: Polyethylene, Waste identification, Plasticresidue, PLS-Rregression, PCAmultivariate analysis, Fourier-transform infrared spectroscopy.

Posted Date: September 23rd, 2021

DOI: https://doi.org/10.21203/rs.3.rs-905784/v1

License: This work is licensed under a Creative Commons Attribution 4.0 International License.
Read Full License

Version of Record: A version of this preprint was published at Journal of Polymers and the Environment on March 7th, 2022. See the published version at https://doi.org/10.1007/s10924-022-02396-3.

Abstract

Low density polyethylene (LDPE) and high density polyethylene (HDPE) are the principal plastics present in solid plastic waste and are found out as the main components of microplastics in marine and terrestrial environments. Currently, efforts have been made to develop new and effective methods to ensure the identification and separation of plastics in waste, ensuring the necessary purity to obtain quality and economically competitive recycled products. In this contribution, we investigated the usage of Fourier-Transform Infrared Spectroscopy in attenuated total reflection mode (ATR-FTIR) combined with Principal Component Analysis (PCA), Linear Partial Least Squares Regression by Intervals (iPLS-R) and Competitive Adaptive Weighted Sampling (CARS/PLS-R) as chemometric methods to classify and determine the compositional fraction of the pristine and recycled mixtures of HDPE and LDPE from plastic waste in São Paulo, Brazil. The 3D PCA plots do not make it possible to classify the different polyethylenes and their polymer blends using the three Principal Components (PC), except for the 2D PCA diagram using PC1 and PC3. The iPLS-R presents the best predictive ability than CARS/PLS-R to determine the LDPE content in HDPE/LDPE recycled blends. However, the presence of different contaminants (in 5 wt%), such as silicon dioxide (SiO_2), calcium carbonate ($CaCO_3$), recycled polypropylene (PP), and recycled poly(ethylene terephthalate) (PET), reduces the potential usage of the iPLS-R models as identification tools for LDPE and HDPE sorting in industrial recycling processes.

1. Introduction

Since the beginning of the 21st century, environmental concerns about global production and inappropriate disposal of plastic residues have been pointed out by the scientific community and regulatory agencies. Among the aggravating points related to the million tons of plastic waste that are in an increasingly worrying state, it stands out the growing need for territorial space for landfilling, crescent consumption of petroleum products, dangerous formation of tiny polymer particles (microplastics) for biological life, carcinogenic and hazardous chemicals in plastic waste [1–5]. Plastics are polymeric materials containing chemical compounds known as additives, which are introduced in the polymer mainly to reduce costs, improve processability, increase or adjust properties to the polymer, and achieve a required performance over a specific application [6].

Low density polyethylene (LDPE) and high density polyethylene (HDPE) are the main polymers present in the plastic waste, followed by polypropylene (PP) and poly(ethylene terephthalate) (PET) [2, 6]. Moreover, polyethylenes (PEs) are the main polymers identified as microplastics in marine and terrestrial environments [7–10], being able to remain in drinking water even after conventional wastewater treatment process [11].

Developed and developing countries have been applied different technological methods and politics for the management of plastic waste as a way to reduce the socio-environmental risks and impacts caused by this type of waste [6, 12–14]. In this way, plastic waste recycling has been used as an eco-friendly option to reinsert plastic residues in industrial production or develop new products from polymer residues.

Mechanical recycling has been widely used to reuse thermoplastic polymer waste in an economically inexpensive manner with a low investment cost, being applied mainly in underdeveloped countries. On the other hand, developed countries, such as the USA, Japan, and European countries, tend to opt for energy recycling which provides an immediate reduction in the volume of plastic waste, but it requires a high financial investment [15–19]. In this context, the recycling situation for polyethylenes is highly worrisome since they are polymer commodities with a relatively low price, accompanied by the high expenses (in cost/kg) for transporting the plastic waste, making their recycled products economically uncompetitive against the price of pristine polyethylenes. Consequently, the recycling processes for revalorization of polyethylene residues are generally considered uneconomic for several recycling industries [5].

Independent of the recycling technology, separation, and sorting of plastic waste play an essential role in obtaining better quality recycled products and optimizing the industrial recycling process [20]. Fourier-Transform Infrared Spectroscopies (FTIR) are attractive vibrational spectroscopies because qualitative and semi-quantitative analyzes can be performed in a non-destructive way. When they are combined with multivariate analysis methods, as chemometric strategies, it is possible to identify and classify rapidly the plastic waste that is suitable to automatize the sorting at industrial scale in recycling processes [21], despite the negative influences caused by the high presence of pigments in black and dark-colored plastic residues [22]. The infrared spectroscopies can also be used to characterize and identify other solid waste types (not only plastic waste) [23] and used to evaluate the aging of plastics [24, 25], a relevant factor that acts on polymeric materials limiting the mechanical recycling of their residues. Moreover, FTIR analysis can be performed in different wavenumber ranges [26]: Near Infrared (NIR, 12800 – 4000 cm^{-1}; Medium Infrared (MIR, 4000 – 400 cm^{-1}); and Far Infrared (FIR, 400 – 10 cm^{-1}). Bekiaris and co-workers [27] successfully predicted the labile fraction of carbon in several composed and non-composed organic waste products using FTIR Photoacoustic Spectroscopy (FTIR–PAS) combined with Principal Component Analysis (PCA) and Partial Least Square Regression (PLS-R). Signoret et al. [28] applied Fourier-Transform Infrared Spectroscopy in attenuated total reflection mode (ATR-FTIR spectroscopy) in MIR spectral region to identify and differentiate various styrenic plastics in Waste of Electric and Electrical Equipment (WEEE). Lenz et al. [29] used FTIR measurements to construct PLS-R regression models as a multivariate analysis tool to control and monitor emissions involving leachate compounds from municipal solid waste (MSW) in landfills. Alassali et al. [30] demonstrated that NIR infrared spectroscopy and PLS-R can be employed to measure quantitatively and accurately the degradation of PE, PP, and PET after different aging conditions but the accuracy of this chemometric method depends on the plastic type. Nunes and co-workers [31] reported that FTIR measurements combined with PCA and PLS-R analyses are appropriate to identify the origin of the olive waste from different mono cultivar olive pomaces and these multivariate analyses present possible application in the quality control of suppliers. Zheng et al. [32] investigated the usage of NIR hyperspectral imaging data processed by PCA statistical method to characterize and sort several plastics in the solid waste, such as polystyrene (PS), PP, PE, PET, and poly(vinyl chloride) (PVC). The authors concluded that the similarity of infrared spectra from the

plastics humper the clustering into distinctive groups, narrowing the application of this procedure to classify unknown plastics in the complex mixture waste.

In summary, PLS-R and PCA are mathematical-statistical methods practical to correlate the concentration of an analyte with a measurable property within a complex system, whose measured responses or analytical signals suffer direct or indirect action of different interference effects, which are intrinsical to the equipment or the measurement method or other physicochemical variables of the system itself [26, 33]. While PLS-R permits predict the analyte content or property of the complex system by a mathematical regression model, PCA enables distinguishing the samples in distinctive groups by the FTIR spectral data decomposition in score plots of the several Principal Components (PCs) [32]. The main advantage of PLS-R is the easy treatment for interpretation of highly correlated data with noise, with physical-chemical interference, and with overlapping signals that are commonly observed in experimental data obtained from vibrational spectroscopies. PLS-R statistical modified versions have been proposed, such as Linear Partial Least Squares Regression by Intervals (iPLS-R) and Competitive Adaptive Weighted Sampling (CARS/PLS-R) [34]. However, few studies reported in the literature involve using these multivariate calibration methods to identify and classify plastic waste [35–37]. iPLS-R is a type of modified PLS-R regression, where the sample spectrum is previously subdivided into smaller equidistant intervals and, subsequently, PLS-R regression is applied to each one. In this way, it is possible to optimize prediction models because subintervals with significant interference or without relevant information can be disregarded, and, generally, iPLS-R models provide more robust prediction models with lower prediction errors [38, 39]. The CARS/PLS-R algorithm was designed to interactively find the most minor “optimal” subset of measured experimental data to obtain the predictive model based on the PLS-R analysis with the lowest error values for prediction by a Monte Carlo sampling method that mimics the biological natural selection process [40].

This work aims to evaluate the potential and limitations associated with the use of ATR-FTIR spectroscopy to classify and analytically determine the compositional fraction of the recycled HDPE/LDPE blends. The PCA chemometric method was used as a classification tool, while iPLS-R and CARS/PLS-R were adopted as quantitative analytical implements. ATR-FTIR spectroscopy combined with multivariate analysis methods is a tool with potential application in the circular economy, being a helpful tool to close the production cycle (through reuse and proper recycling) of packaging, electronics, and automobile parts manufactured with mixtures of polyethylenes.

2. Materials Ad Methods

2.1. Materials

Pristine LDPE (MFI of 2.6 g/10 min, 190°C, 2.16 kg) and pristine HDPE (MFI of 0.3 g/10 min, 190°C, 5 kg) were obtained from Braskem and Petroquímica Triunfo S.A., respectively. Recycled LDPE (MFI of 9.5 g/10 min, 190°C, 2.16 kg), recycled HDPE (MFI of 0.8 g/10 min, 300°C, 1.2 kg), recycled PET (MFI of 14 g/10 min, 255°C, 2.16 kg), and recycled PP (MFI of 0.5 g/10 min, 230°C, 2.16 kg) were obtained from NZ

Cooperpolymer (São Paulo, Brazil). All the melt flow index (MFI) results were determined according to ASTM D-1238. All recycled polymers are from the mechanical recycling of polymeric post-consumer waste from São Paulo, Brazil. In addition, calcium carbonate (400 mesh, aperture size = 37 μm) and silica gel (particle diameter in the range 40–60 μm) were purchased from Brasilminas and Merck, respectively.

2.2. Sample preparation

The pristine and recycled HDPE/LDPE blends were prepared in the Dynisco extruder (heating zones operating at 190 and 200°C; screw rotation speed equal to 220 rpm), using twenty-one different compositions from 0 to 100 wt% of HDPE. Recycled PET, recycled PP, powdered silica (SiO_2), and powdered calcium carbonate ($CaCO_3$) were used as known contaminants in this research work. For this purpose, these materials were added to the HDPE/LDPE polymeric blends based on the recycled polyethylenes (known contaminant content fixed on 5 wt%). Only the recycled HDPE/LDPE blends with PET were extruded with heating zones operating at 220 and 230°C, corresponding to the minimum temperature range for plasticizing and processing PET.

2.3. Characterizations

2.3.1. Scanning electron microscopy (SEM) and x-ray dispersive energy spectroscopy (EDS)

The SEM micrographs and the elementary analyzes by EDS spectroscopy were obtained by a Field Emission Gun Scanning Electron Microscope (FEI Company, model FEG - Inspect F50). For this, the polymers were covered with gold (thickness from 5 to 10 nm).

2.3.2. Surface roughness by SEM

The SEM micrographs of the surface of the samples, in the form of pellets, were performed in the scanning electron microscope (FEI Company, model FEG - Inspect F50). The samples were covered with gold (film with a thickness of 5 to 10 nm), using a BALZERS - SCD050 (BALTEC) table sprayer with a deposition time of 25 seconds. SEM micrographs (2000 times magnification) were made with secondary electrons, using a working distance of 11.14 mm and an angle of 90 ° between the electron beam and the sample. The mean quadratic roughness (R_q) was also obtained with the ImageJ program, but the micrographs were digitized in 32-bit grayscale, and the roughness was determined by the SurfCharJ plugin developed by Chinga and collaborators [41].

2.3.3. Thermogravimetric analysis (TGA)

The thermal decomposition profiles of the polymers were identified by a thermogravimetric analyzer (TGA/SDTA 851e, Mettler Toledo. The samples were heated from 25 to 600°C at the rate of 10°C min^{-1} under a continuous flow of N_2 (50 mL min^{-1}).

2.3.4. Attenuated Total Reflectance - Fourier Transform Infrared Absorption Spectroscopy (ATR-FTIR)

ATR-FTIR spectra of the HDPE/LDPE pellets were collected by an ATR accessory (ZnSe crystal) on a Thermo IS5 Nicolet spectrometer and collected from 600 to 4000 cm^{-1} at room temperature, 16 scans and spectral resolution of 4 cm^{-1}.

2.3.5. Software, multivariate analysis, and data treatment

All ATR-FTIR data were smoothed using the Savitzky-Golay method [42], using polynomial order of 5 and window points of 10. Subsequently, the ATR-FTIR spectra were normalized before the multivariate analysis procedure. As an ordination method, PCA was carried out in Past4.01 software and Principal Component Analysis Tool v1.50 (MATLAB R2018b). CARS/PLS-R regressions pre-processed spectra were performed on MATLAB software (version R2015a) using libPLS 1.95 toolbox [43]. iPLS-R regressions were carried out in MATLAB (R2015a) environment using the iToolbox package [44]. The ATR-FTIR data from the recycled HDPE/LDPE blends without known contaminants were applied as a cross-validation set for the iPLS-R, while the spectral data from the contaminated recycled HDPE/LDPE blends were used as an independent prediction set.

For the iPLS-R algorithm, all the ATR-FTIR spectra were segmented in 30 equidistant intervals, processed using the autoscaling method, and the selected spectral region for the iPLS-R corresponds from 2800 to 3000 cm^{-1}. In contrast, the mean centering pretreatment method was used before the CARS/PLS-R multivariate analyses (constant parameters: cross-validation = 15; the maximal number of latent variables for cross-validation = 20). These were the best conditions for iPLS-R and CARS/PLS-R regressions achieved in previous works involving the HDPE/LDPE polymeric system [35, 36]. Figure 1 illustrates the procedure for the sample preparation, characterization, and ATR-FTIR data analysis using PCA and PLS-R multivariate analyses.

As a way to assess the performance and generality of prediction from PLS-R models, statistical parameters of mean cross-validation square error (RMSECV) and mean prediction square error (RMSEP) are used and calculated by Eq. (1) [35, 45].

$$RMSECV/P = \sqrt{\frac{\sum_{i=1}^{z}\left(y_i - \hat{y}_i\right)^2}{z}} \quad (1)$$

where z is the number of spectra, y_i is the reference LDPE concentrations for the sample *i*, and $\hat{y}_i$ is the predicted LDPE concentration of the sample in the calibration set (RMSECV) or the independent validation test set (RMSEP).

The adjustment degree between the predicted values and the reference values calculated by the PLS-R methods is assessed by the correlation coefficient (*R*), given by Eq. (2) [37].

$$R = \sqrt{1 - \frac{\sum_{i=1}^{z} \left(y_i - \hat{y}_i\right)^2}{\sum_{i=1}^{z} \left(y_i - \hat{y}_{mean}\right)^2}}$$

2

where $\hat{y}_{mean}$ is the average result for the reference LDPE concentration of all samples in the cross-validation set (R_{cal}) or the independent/external validation set (R_{pred}).

3. Results And Discussion

3.1. SEM and EDS analyses

In the SEM micrographs of the recycled HDPE (Fig. 2), it is possible to identify impurities on the surface of this polymer. The EDS spectra indicate that these contaminants are constituted by K, O, Si, Na, Mg, Fe, S, Cl, Ca, and P chemical elements. These chemical elements can be related to different additives present in HDPE, as detailed in Table 1 [46–49]. The presence, in greater concentration, of carbon is due to the chemical composition of the PE polymer chains. Besides being associated with the additives mentioned previously, the oxygen element can also be associated with oxidative degradation of the polymer during its processing and life service time. These EDS elemental signals cannot be associated with residual Phillips catalyst (based on chromium oxide) supported on silica or alumina and residual Ziegler-Natta catalysts based on alkyl aluminum compounds and a salt (containing Ni, Co, Zr, or Ti) [50] due to their low residual concentrations for the synthesis of HDPE, since these chemical elements were not identified in the pristine HDPE. According to TGA results (Supplementary Material), the impurity content in the recycled polyethylenes is very low since the carbonaceous residues were 0.72 wt% and 0.78 wt% for pristine and recycled LDPE, respectively. At the same time, the residual mass is 0.68 wt% for pristine HDPE and 0.98 wt% for recycled HDPE. Moreover, the recycled and pristine polyethylenes present a similar mass loss curve with a single thermo-decomposition process with maximum rate, indicating the absence of another type of polymer in the recyclates.

The recycled LDPE also has impurities, as shown in Fig. 3, composed of Al, Fe, Mg, O, and Si. These elements are typical chemical constituents of silicates [51]. Since particle size is in the micrometer order, these silicates were probably applied as a filler or come from contamination after the disposal of the LDPE-based product. However, LDPE is typically used to manufacture food packaging, and nanometric clays can be introduced in LDPE and other polymer films to reduce oxygen gas diffusion into the product due to a barrier effect [52], reducing the speed oxidation of packaged food. In addition, nano-clays are used as reinforcement fillers in polymers, being widely applied in the development of polymer matrix nanocomposites [53, 54].

Table 1
Possible additives present in recycled PEs associated with the chemical elements detected by EDS.

Chemical element	Polymer additives
P, O, and S	Phosphates, phosphites, and sulfites are secondary antioxidants, acting on the decomposition of hydroperoxides that are formed in the plastic
Mg, O, and Si	Talc (filler) containing magnesium oxide (MgO), silicon dioxide (SiO_2), and adsorbed water
Ca, C and O	Calcium carbonate ($CaCO_3$), which is a filler typically used as a filler in polymers, to lower the price of the plastic product
Si and O	Silicon dioxide (SiO_2) and glass are used as fillers and reinforcement in thermoplastics.
Cl	Presence of chlorinated flame retardants or presence of chlorinated compounds in recycled HDPE due to its direct contact with chlorinated drinking water, when this polymer is used as tubes
Fe, Na, K, Si, Mg, and O	Mica and clays (silicates) are commonly used as fillers in the granulometry observed in the recycled HDPE micrograph

3.2. ATR-FTIR spectroscopy

The ATR-FTIR spectra of HDPE and LDPE, pristine and recycled, are shown in Fig. 4. The vibration band located at 705–735 cm^{-1} corresponds to the deformation in the plane (per rotation) of the connections in the methylene group (amorphous phase and crystalline). The balance-type deformations of the C-H bonds in the amorphous and crystalline phases are associated with the signal at 1450–1480 cm^{-1}. The signal at 2875 – 2770 cm^{-1} is related to the symmetrical stretching of CH_2 (amorphous and crystalline phases), while the vibrational band at 2980 – 2875 cm^{-1} refers to the asymmetric stretching of CH_2 (amorphous phase). The absorption bands with low intensity at 1306–1351 cm^{-1} were observed and are connected with the out-of-plane deformations (torsion and swing type) of the CH_3 groups. A weak absorption at 1340–1390 cm^{-1} is observed in the polyethylene spectra, also due to the balance-type deformation of the CH_3 groups [55–59]. The main differences between the ATR-FTIR spectra from HDPE and LDPE correspond to variations in the absorption intensity of infrared radiation in the 1450–1480 cm^{-1} and 2980 – 2875 cm^{-1} bands. Also, there are differences in the ATR-FTIR spectra region at 1340–1390 cm^{-1}. These infrared alterations are associated with the differences in the content of amorphous and crystalline phases occasioned by the increase of CH_3 groups in LDPE due to the highest quantity of polymer branches in this polyethylene type than in HDPE [60].

The characteristic absorption signals for the chemical groups and their vibrational modes in PP [61], PET [62–64], silica (SiO_2) [65], and calcium carbonate ($CaCO_3$) [63, 66] from the ATR-FTIR spectra (Fig. 5) are detailed in Table 2. The FTIR spectrum from recycled PET does not indicate the presence of functional

groups due to the presence of contaminants. Vaterite (space group Pbnm), calcite (space group $R\bar{3}C$ and aragonite (space group Pmcn) are the three $CaCO_3$ polymorphic crystalline phases based on hexagonal, trigonal, and orthorhombic crystal systems, in that order [67, 68]. Silicon dioxide (silica) also displays polymorphic behavior, presenting eight different crystalline phases containing a different number of SiO_2 groups per unit cell [69]: α-quartz (trigonal cell unit with space group $P3_221$), α-cristobalite (tetragonal cell unit with space group $P4_12_12$), α-tridymite (orthogonal cell unit with space group $C222_1$), coesite (monoclinic cell unit with space group C2/c), keatite (tetragonal cell unit with space group $P4_32_12$), tridymite (hexagonal cell unit with space group $P6_3/m\ mc$), β-quartz (hexagonal cell unit with space group $P6_222$), and β-cristobalite (cubic cell unit with space group Fd-3m). Highlighting that calcite and α-quartz are the crystalline phases most stable at ambient temperature and pressure conditions, while the space group of vaterite is not well established in the literature [70]. The ATR-FTIR spectra suggest the calcite phase in the $CaCO_3$ particles due to characteristic absorption bands at 874 and 2512 cm^{-1}.

Table 2
ATR-FTIR characteristic signals of the polymers, silicon dioxide, and calcium carbonate (part I).

Polymer	Wavenumber (cm^{-1})	Chemical group and vibrational mode
HDPE and LDPE (pristine and recycled)	718	-CH_2- (Rocking)
	730	-CH_2- (Rocking)
	1306	-CH_3 (Twisting and wagging)
	1350	-CH_3 (Twisting and wagging)
	1367	-CH_3 (Wagging)
	1460	-CH- (Bending)
	2850	-CH_2- (Symmetric stretching)
	2920	-CH_2- (Asymmetric stretching)
PP	808	C–C (Stretching)
	840	-CH- (Rocking)
	973	-CH_3 (Rocking) C–C (Stretching)
	996	CH_3 (Rocking)
	1166	C–C (Stretching) -CH- (Wagging) -CH_3 (Rocking)
	1376	-CH_3 (Symmetric bending)
	1456	-CH_3 (Symmetric bending)
	2870	-CH_3 (Stretching)
	2920	-CH_2- (Asymmetric stretching)
	2950	-CH_3 (Asymmetric stretching)
SiO_2	796	Si-O-Si (Symmetrical stretching)
	975	Si-O-(H-H_2O) (Bending)
	1060	Si-O-Si (Asymmetrical stretching)

Polymer	Wavenumber (cm^{-1})	Chemical group and vibrational mode
	3447	- O-H from SiOH and adsorbed H_2O (Stretching)

HDPE, LDPE, and PP recyclates seem to have a low degradation degree since there is not infrared signal at 1170 and 1167 cm^{-1}, corresponding to the formation of C-O (carbonyl) from ester groups due to the aging of polyolefin residues after their end-of-life and mechanical recycling steps [24].

Table 2
ATR-FTIR characteristic signals of the polymers, silicon dioxide, and calcium carbonate (continuation).

Material	Wavenumber (cm^{-1})	Chemical group and vibrational mode
PET	721	Interactions between polar ester groups and benzene rings
	794 and 848	Vibrations of adjacent two aromatic H in p-substituted rings
	874 and 973	Vibrations of adjacent two aromatic H in 1,2,4,5-tetrasubstituted aromatic rings (in- and out-of-plane bendings)
	1042 and 1092	Vibrations of methylene group and C-O in ester groups
	1119 and 1247	Vibrations of terephthalate group ($OOCC_6H_4$-COO)
	1344, 1411 and 1457	C-O (Stretching) O-H (bending and wagging)
	1504 and 1577	C = C and C–H of phenyl rings (Vibrations of the aromatic rings with stretching)
	1715	C = O of the carboxylic acid groups (Stretching)
	1960	Vibrations of aromatic rings
	2350	CO_2 (Axial symmetrical deformation)
	2969	C–H (Symmetrical stretching)
	3054	CH aromatic rings (Symmetric stretching)
$CaCO_3$	708	CO_3 (Stretching)
	874	C-O from calcite
	1409–1460	C = O (Asymetric stretching) O-H (Bending)
	1805	Vibrations of carbonate ions
	2512	C = O from calcite

The remarkable intensity of the C = O stretching vibration from carboxylic acid groups at wavenumber 1715 cm^{-1} indicates that the PET recyclates present a high degradation degree [24, 71], justifying the elevated value for the MFI (14 g/10 min at 255°C) of the recycled PET. During the mechanical recycling, PET residues can degrade by thermal-oxidative and hydrolytic action combined with water and oxygen molecules, both involving breaking the ester bonds between the terephthalic acid and diethylene glycol units along the polymer backbones. The thermal-oxidative degradation leads to rupture of the polymeric chains, forming carboxyl acid and vinyl ester end groups in the PET. On the other hand, hydrolysis also causes the PET polymer chains, but carboxyl acid and hydroxyl ester end groups are generated by this degradation process [72].

3.3. Principal component analysis (PCA)

The 2D and 3D diagrams of the PC scores obtained by the PCA statistical analysis of the ATR-FTIR data from the pristine and recycled polyethylenes are presented in Fig. 6. The PC1 and PC2 scores correspond to 72.9 % and 8.6 % of the variance among the infrared spectral data from the polyethylenes, respectively. However, the PC scores do not enable the complete distinction of the pristine and recycled polyethylenes without the 5 wt% of contaminants (pHDPE, pLDPE, rHDPE, and rLDPE samples) due to the overlap of the 95 % confidence ellipses. Moreover, the PC1 score evidently has less representativeness over the ATR-FTIR spectra of LDPE. In contrast, the PCA plot using de PC1 and PC3 scores permitted the separation of some plastics, such as pristine polyethylenes, pristine HDPE and recycled LDPE (with or without 5 wt% of contaminants). Also, the contaminant presence reduces the confidence ellipse area for the recycled HDPE, enabling a more effective separation between the recycled HDPE and the samples containing LDPE.

The first three PC scores (PC1, PC2, and PC3) from PCA analysis represent 76.1 % of the total variability for the HDPE/LDPE blends based on recycled and pristine plastics, as can be seen in Fig. 7. Obviously, the addition of the contaminants modifies the format of the confidence ellipses, but the recycled and pristine HDPE/LDPE without contaminants present a similar confidence ellipse. The presence of 5 wt% of silica in the recycled HDPE/LDPE substantially increases the variation of the calculated PC scores, and consequently, the confidence ellipse area is enlarged. According to the 2D diagrams in Fig. 8, the PC1 and PC2 scores do not make it possible to separate the HDPEs, LDPEs, and HDPE/LDPE blends effectively since the groups are not clustered by the PCA analysis, indicating a high similarity of their ATR-FTIR spectra [32].

3.4. Partial Least Squares Linear Regression modified by Competitive Adaptive Reweighted Sampling (CARS/PLS-R)

The value obtained for RMSEP for the CARS-/PLS-R model is very high (Fig. 9), equal to 39.712 wt% of LDPE, and the value of R_{pred} is equal to 0.331. The predicted results form a straight line with an inclination equal to 1, but with a linear coefficient other than zero as a constant value shifted the model's prediction line, 40 wt% of LDPE, concerning the regression line (built in the multivariate calibration of the CARS/PLS-R prediction model). According to Miller et al. [73], this type of non-agreement between

calibration and prediction values may be connected with systematic or random errors in the spectrometer's background signal. Therefore, this high discrepancy suggests that the CARS/PLS-R model is susceptible to slight variations in ATR-FTIR spectral signals related to the heterogeneity of recycled plastics. The high prediction error and low calibration error for the CARS/PLS-R predictive model indicate that the CARS/PLS-R multivariate calibration method can obtain highly calibrated predictive models with low capacity to predict the LDPE content in plastic waste containing HDPE and LDPE mixtures.

The low performance of the CARS/PLS-R model is also associated with the increase in the surface irregularity of the recyclates' pellets since HDPE increases the viscosity of the HDPE/LDPE blend in the molten state because HDPE has a lower melt flow index than the LDPE at the same temperature. The rise in melt viscosity of HDPE, LDPE, and HDPE/LDPE polymer systems intensifies the shear rate on the surface of the molten material during its passage in the extruder matrix and, consequently, there is the formation of surface defects due to plastic deformation in the extruded polymer. If the shear stress in the extruder matrix is much higher than the melt strength, the defects are no longer superficial and the melt fracture, which is a macroscopic defect, occurs. In addition, the elevation in melt viscosity results in more outstanding adhesion with the machinery, which also intensifies the occurrence of surface defects and fracture of the cast of the extruded profile. In addition, the mixtures of HDPE with LDPE can form immiscible multiphase systems in which there are morphological changes (e.g., deformation, rupture, and coalescence) and interfacial processes (e.g., interfacial relaxation and sliding) between the dispersed polymer droplets and the polymeric matrix under stress shear; both phenomena significantly influence the HDPE/LDPE melt flow within the extruder matrix, leading to changes on the extrudate surface [74–77].

As the ATR-FTIR spectroscopy analyses are performed on the samples' surface, it is of great importance to evaluate their surface roughness. Thus, the R_q roughness of the HDPE and LDPE mixtures was determined from SEM micrographs using computational analysis. This type of essay is based on local brightness variations in the SEM micrograph (i.e., changes in grayscale uniformity) directly associated with the topography of the sample [41, 78]. According to Fig. 10, the R_q roughness results of the HDPE pellets are 100 % higher than R_q values for the LDPE pellets, independently of the plastics being recycled or pristine even though these plastics were extruded under similar conditions. Thus, R_q roughness emphasizes the weight of the topographical peaks and valleys in the results of the surface roughness. It is observed in Fig. 10a that the roughness of the pellets of the pristine LDPE/HDPE blends increases as the HDPE concentration increases in the polymer mixture. When the HDPE content is equal to or higher than 50 wt%, there is a significant increase (> 25%) in the R_q roughness of the pellets of recycled LDPE/HDPE blends (Fig. 10b).

3.5. Partial Least Squares Linear Regression (iPLS-R)

The iPLS-R algorithm found the minimum calibration and prediction errors in the range of 2875–2980 cm^{-1} to construct the iPLS-R model, suggesting a close relationship between composition and the amorphous fraction of the HDPE/LDPE blends. The results of the prediction test of the iPLS-R model are

shown in Fig. 11. As can be identified, the RMSEP error is equal to 6.479 wt% of LDPE, and the R_{pred} is 0.995, while there is a low adjustment factor for the recycled blends containing less than 10 wt% of LDPE.

Due to the highest predictive performance, the predictive capability of this iPLS-R model to determine the composition of polymeric blends of recycled HDPE/LDPE containing other materials in its composition was evaluated. In this work, we chose the contaminant concentration of 5 wt% for PP, PET, calcium carbonate and silica, since PP and PET are two of the most present thermoplastics in solid urban waste generated worldwide. Calcite and silica are often used in polymers as fillers to improve the dimensional stability of plastic products to reduce the product's final cost, as these inorganic materials are generally cheaper than the polymers available on the market. The ATR-FTIR spectra of the uncontaminated and contaminated HDPE/LDPE blends obtained with the recycled plastics are present in Supplementary Material.

As shown in Fig. 11, the prediction errors of the iPLS-R model increase significantly when the HDPE/LDPE blends present this percentage of contamination, mainly with PET, PP, and carbonate of calcium in recycled polymer blends. The minor prediction error was obtained in tests involving polymeric blends with silica gel (RMSEP = 7.771 wt% of LDPE) and a prediction error exceeding 16 wt% of LDPE when the plastic samples contain the other three contaminants investigated in this work. In addition, the pronounced calibration and prediction errors are also associated with the increase in the surface roughness of the plastic pellets (Fig. 12). The increase of the surface roughness of the polyethylene pellets due to the elevation of the viscosity of the plastic melt, which is caused by contaminant addition in the recycled polyethylene, leads to more significant uncertainty in the ATR-FTIR spectral measurements.

According to Fig. 13, there is a significant increase in the roughness of the recycled LDPE pellets when it is used silica and PP as contaminants. Silica and calcium carbonate substantially increase the roughness of the recycled HDPE, while PET and PP seem not to affect it. This phenomenon is because the contaminants (principally SiO_2 and $CaCO_3$) decrease substantially the melt fluidity of the PE-based systems, increasing their viscosity in the molten state, and consequently, the pellets' roughness is raised as discussed so far.

3.6. Final remarks

Automatized and efficient processes to classify plastics are essential for the recycling industry to improve the recycling of the principal plastics in the waste generated worldwide. However, there are several difficulties in producing recycled polyethylene residues with technologically attractive properties and competitive prices, such as, for example, the degradative processes that act on the polymer (during and after its lifetime) and the presence of contaminants that often prevents the separation of solid polymeric waste (SPWs) [17, 79]. In addition, the quality control of the separation step, that is, assessing the purity degree of the different plastics separated to be mechanically recycled, plays a fundamental role in obtaining good quality recycled plastic products. However, quantifying the composition of mixtures of

HDPE with LDPE is not a simple task since they are only constituted by hydrogen and carbon atoms connected by saturated chemical bonds.

In Brazil and other underdeveloped countries, plastics are recycled mainly by mechanical recycling, which is the most used process to reuse plastic residues [57]. However, the complete separation of the mixtures of HDPE and LDPE residues by the method of density difference, using alcoholic and aqueous solutions, after manual separation, is challenging. In addition, the presence of fillers (and other additives), plastic mixtures, and multilayer polymeric packaging in the plastic waste make this conventional sorting method unfeasible [80]. It is worth mentioning that this separation procedure is currently the cheapest and, consequently, it is the most used for the separation of polyolefin waste in the mechanical recycling process in Brazil [50].

Another aggravating factor for the proper identification and separation of plastics in polymeric packaging waste by regulatory laws. In Brazil, the correct identification of plastic-type in solid plastic waste by ABNT NBR 13.230 does not exceed 30 % of the total food and non-food products sold on the market [81], making the processes characterization and sorting involved in plastic recycling even more difficult.

In our work, the identification of polyethylene recyclates using ATR-FTIR spectroscopy combined with PCA and different PLS-R statistical analyses were investigated in-depth. This methodology would be helpful for the online characterization and sorting of plastic pieces in a large-scale recycling process involving solid plastic waste. However, several limitations were identified in this proposed procedure due to the great complexity associated with the heterogeneity observed for plastic residues, which affect the ATR-FTIR signal associated both by the composition and the surface morphology of the sample.

The objective of the present work was to point out the applicability and the barriers to the usage of the ATR-FTIR spectroscopy, which is a technique that makes it possible to characterize analytically and quickly solid samples, such as solid plastic waste, being suitable to be applied in different industrial sectors. The PCA and PLS-R multivariate analyses show appropriate development of fast, analytical, and automated protocols for classifying polyethylenes and determining the LDPE content in HDPE/LDPE mixtures using infrared measurements. However, the presence of 5 wt% of a contaminant such as another polymer with different chemical composition or microparticles of oxides restricts the capacity and generality of the PCA and PLS-R statistical models for sorting highly heterogeneous mixtures of plastic residues found in real plastic waste. Despite these limitations, the analytical iPLS method proposed here presents more excellent reliability for mixtures of LDPE/HDPE with silica impurities under the evaluated conditions of tests. The PCA method using the PC1 and PC3 plot can be helpful to separate pristine and recycled LDPE and HDPE, depending on the waste composition, showing a latent capacity to be applied as a tool to identify polyethylene-based plastic packages and support the management of the circular economy processes.

4. Conclusions

In this paper, PLS-R and PCA multivariate analyses were investigated for the ATR-FTIR identification and sorting of different mixtures of recycled HDPE and LDPE with or without PP, PET, silica gel, and calcium carbonate applied as known contaminants. The HDPE, LDPE, and their mixtures were not clustered into distinct groups using their ATR-FTIR spectral characteristic signals using PC1 and PC2 scores in two-dimensional and three-dimensional PCA plots. Only the PCA plot with PC1 and PC3 scores enables grouping the pristine LDPE and pristine HDPE, as well as recycled polyethylene mixtures with 5 wt% of the known contaminants for identification and separation of these plastics.

The HDPE and LDPE recycled plastics have different impurities but in low concentrations (< 1 wt%). In tests using ATR-FTIR spectral data from recycled HDPE/LDPE blends containing 5 wt% of PP, PET, silica, and calcium carbonate, the predictive models based on iPLS-R showed prediction errors between 11 wt% and 19 wt% of LDPE in the whole LDPE content range (from 0 to 100 wt%). Only for samples containing silica, the iPLS-R predictive model exhibited RMSEP close to 9 wt% of LDPE. iPLS-R enables quantifying the composition of recycled HDPE/LDPE blends containing contaminants (in 5 wt%) in the whole LDPE content range (0–100 wt%) a root mean square error below 7 wt%. This paper shows that the CAR/PLS-R approach does not guarantee effective classification and correct composition determination of HDPE and LDPE mixtures in plastic waste.

5. Declarations

Acknowledgment

This study was financed in part by the Coordenação de Aperfeiçoamento de Pessoal de Nível Superior – Brasil (CAPES) – Finance Code 001. The authors are grateful to NZ Cooperpolymer for donating polymeric recycled materials

6. References

1. Geyer R, Jambeck JR, Law KL (2017) Production, use, and fate of all plastics ever made. Sci Adv 3:e1700782. doi: 10.1126/sciadv.1700782
2. Diaz Silvarrey LS, Phan AN (2016) Kinetic study of municipal plastic waste. Int J Hydrogen Energy 41:16352–16364. doi: 10.1016/j.ijhydene.2016.05.202
3. Cole M, Lindeque P, Halsband C, Galloway TS (2011) Microplastics as contaminants in the marine environment: A review. Mar Pollut Bull 62:2588–2597. doi: 10.1016/j.marpolbul.2011.09.025
4. Pivnenko K, Eriksen MK, Martín-Fernández JA, et al (2016) Recycling of plastic waste: Presence of phthalates in plastics from households and industry. Waste Manag 54:44–52. doi: 10.1016/j.wasman.2016.05.014
5. Horodytska O, Valdés FJ, Fullana A (2018) Plastic flexible films waste management – A state of art review. Waste Manag 77:413–425. doi: 10.1016/j.wasman.2018.04.023

6. Eriksen MK, Pivnenko K, Olsson ME, Astrup TF (2018) Contamination in plastic recycling: Influence of metals on the quality of reprocessed plastic. Waste Manag 79:595–606. doi: 10.1016/j.wasman.2018.08.007
7. Andrady AL (2017) The plastic in microplastics: A review. Mar Pollut Bull 119:12–22. doi: 10.1016/j.marpolbul.2017.01.082
8. Zhang S, Wang J, Liu X, et al (2019) Microplastics in the environment: A review of analytical methods, distribution, and biological effects. TrAC Trends Anal Chem 111:62–72. doi: 10.1016/j.trac.2018.12.002
9. Zhou Y, Wang J, Zou M, et al (2020) Microplastics in soils: A review of methods, occurrence, fate, transport, ecological and environmental risks. Sci Total Environ 748:141368. doi: 10.1016/j.scitotenv.2020.141368
10. Sarker A, Deepo DM, Nandi R, et al (2020) A review of microplastics pollution in the soil and terrestrial ecosystems: A global and Bangladesh perspective. Sci Total Environ 733:139296. doi: 10.1016/j.scitotenv.2020.139296
11. Sun J, Dai X, Wang Q, et al (2019) Microplastics in wastewater treatment plants: Detection, occurrence and removal. Water Res 152:21–37. doi: 10.1016/j.watres.2018.12.050
12. Barros NG de (2013) Propriedades de material polimérico obtido da reciclagem de embalagens multicamadas. Universidade Estadual de Campinas
13. Milios L, Holm Christensen L, McKinnon D, et al (2018) Plastic recycling in the Nordics: A value chain market analysis. Waste Manag 76:180–189. doi: 10.1016/j.wasman.2018.03.034
14. Van Eygen E, Laner D, Fellner J (2018) Circular economy of plastic packaging: Current practice and perspectives in Austria. Waste Manag 72:55–64. doi: 10.1016/j.wasman.2017.11.040
15. Singh N, Hui D, Singh R, et al (2017) Recycling of plastic solid waste: A state of art review and future applications. Compos Part B Eng 115:409–422. doi: 10.1016/j.compositesb.2016.09.013
16. Mekhzoum M, Benzeid H, Rodrigue D, et al (2017) Recent Advances in Polymer Recycling: A Short Review. Curr Org Synth 14:171–185. doi: 10.2174/1570179413666160929095017
17. Al-Salem SM, Lettieri P, Baeyens J (2009) Recycling and recovery routes of plastic solid waste (PSW): A review. Waste Manag 29:2625–2643. doi: 10.1016/j.wasman.2009.06.004
18. Kumar A, Samadder SR (2017) A review on technological options of waste to energy for effective management of municipal solid waste. Waste Manag 69:407–422. doi: 10.1016/j.wasman.2017.08.046
19. da Silva DJ, Wiebeck H (2020) Current options for characterizing, sorting, and recycling polymeric waste. Prog Rubber, Plast Recycl Technol 36:284–303. doi: 10.1177/1477760620918603
20. Hopewell J, Dvorak R, Kosior E (2009) Plastics recycling: challenges and opportunities. Philos Trans R Soc B Biol Sci 364:2115–2126. doi: 10.1098/rstb.2008.0311
21. Vrancken C, Longhurst PJ, Wagland ST (2017) Critical review of real-time methods for solid waste characterisation: Informing material recovery and fuel production. Waste Manag 61:40–57. doi:

10.1016/j.wasman.2017.01.019

22. Junjuri R, Gundawar MK (2020) A low-cost LIBS detection system combined with chemometrics for rapid identification of plastic waste. Waste Manag 117:48–57. doi: 10.1016/j.wasman.2020.07.046
23. Smidt E, Meissl K, Schwanninger M, Lechner P (2008) Classification of waste materials using Fourier transform infrared spectroscopy and soft independent modeling of class analogy. Waste Manag 28:1699–1710. doi: 10.1016/j.wasman.2007.08.003
24. Signoret C, Edo M, Caro-Bretelle A-S, et al (2020) MIR spectral characterization of plastic to enable discrimination in an industrial recycling context: III. Anticipating impacts of ageing on identification. Waste Manag 109:51–64. doi: 10.1016/j.wasman.2020.04.043
25. Alassali A, Picuno C, Bébien T, et al (2020) Validation of near infrared spectroscopy as an age-prediction method for plastics. Resour Conserv Recycl 154:104555. doi: 10.1016/j.resconrec.2019.104555
26. Medeiros ARB de (2009) Uso de ATR/FTIR e FTNIR associado a técnicas quimiométricas para quantificação de aditivos em gasolina automotiva. Universidade de Brasília
27. Bekiaris G, Bruun S, Peltre C, et al (2015) FTIR–PAS: A powerful tool for characterising the chemical composition and predicting the labile C fraction of various organic waste products. Waste Manag 39:45–56. doi: 10.1016/j.wasman.2015.02.029
28. Signoret C, Caro-Bretelle A-S, Lopez-Cuesta J-M, et al (2019) MIR spectral characterization of plastic to enable discrimination in an industrial recycling context: I. Specific case of styrenic polymers. Waste Manag 95:513–525. doi: 10.1016/j.wasman.2019.05.050
29. Lenz S, Böhm K, Ottner R, Huber-Humer M (2016) Determination of leachate compounds relevant for landfill aftercare using FT-IR spectroscopy. Waste Manag 55:321–329. doi: 10.1016/j.wasman.2016.02.034
30. Alassali A, Fiore S, Kuchta K (2018) Assessment of plastic waste materials degradation through near infrared spectroscopy. Waste Manag 82:71–81. doi: 10.1016/j.wasman.2018.10.010
31. Antónia Nunes M, Páscoa RNMJ, Alves RC, et al (2020) Fourier transform near infrared spectroscopy as a tool to discriminate olive wastes: The case of monocultivar pomaces. Waste Manag 103:378–387. doi: 10.1016/j.wasman.2019.12.050
32. Zheng Y, Bai J, Xu J, et al (2018) A discrimination model in waste plastics sorting using NIR hyperspectral imaging system. Waste Manag 72:87–98. doi: 10.1016/j.wasman.2017.10.015
33. Gomes ADA (2012) Algoritmo das Projeções Sucessivas aplicado à seleção de variáveis em regressão PLS. Universidade Federal da Paraíba
34. Rocha JTC, Oliveira LMSL, Dias JCM, et al (2016) Sulfur Determination in Brazilian Petroleum Fractions by Mid-infrared and Near-infrared Spectroscopy and Partial Least Squares Associated with Variable Selection Methods. Energy and Fuels 30:698–705. doi: 10.1021/acs.energyfuels.5b02463
35. da Silva DJ, Wiebeck H (2017) Using PLS, iPLS and siPLS linear regressions to determine the composition of LDPE/HDPE blends: A comparison between confocal Raman and ATR-FTIR spectroscopies. Vib Spectrosc 92:259–266. doi: 10.1016/j.vibspec.2017.08.009

36. da Silva DJ, Wiebeck H (2018) CARS-PLS regression and ATR-FTIR spectroscopy for eco-friendly and fast composition analyses of LDPE/HDPE blends. J Polym Res 25:112. doi: 10.1007/s10965-018-1507-5
37. Silva DJ da, Wiebeck H (2019) Predicting LDPE/HDPE blend composition by CARS-PLS regression and confocal Raman spectroscopy. Polímeros 29:e2019010. doi: 10.1590/0104-1428.00218
38. Silva FEB, Flores ÉMM, Parisotto G (2016) Green method by diffuse re fl ectance infrared spectroscopy and spectral region selection for the quanti fi cation of sulphamethoxazole and trimethoprim in pharmaceutical formulations. An Acad Bras Cienc 88:1–15. doi: 10.1590/0001-3765201620150057
39. Zuo X, Fang S, Liang X (2014) Synergy interval Partial Least Square (siPLS) with potentiometric titration multivariate calibration for the simultaneous determination of amino acids in mixtures. Adv J Food Sci Technol 6:1209–1218.
40. Li H, Liang Y, Xu Q, Cao D (2009) Key wavelengths screening using competitive adaptive reweighted sampling method for multivariate calibration. Anal Chim Acta 648:77–84. doi: 10.1016/j.aca.2009.06.046
41. CHINGA G, JOHNSEN PO, DOUGHERTY R, et al (2007) Quantification of the 3D microstructure of SC surfaces. J Microsc 227:254–265. doi: 10.1111/j.1365-2818.2007.01809.x
42. Savitzky A, Golay MJE (1964) Smoothing and Differentiation of Data by Simplified Least Squares Procedures. Anal Chem 36:1627–1639. doi: 10.1021/ac60214a047
43. Li H, Xu Q, Liang Y (2014) libPLS: An Integrated Library for Partial Least Squares Regression and Discriminant Analysis. PeerJ Prepr 2:e190v1. doi: 10.7287/peerj.preprints.190v1
44. Nørgaard L, Hahn MT, Knudsen LB, et al (2005) Multivariate near-infrared and Raman spectroscopic quantifications of the crystallinity of lactose in whey permeate powder. Int Dairy J 15:1261–1270. doi: 10.1016/j.idairyj.2004.12.009
45. Ferrão MF, Viera MDS, Pazos REP, et al (2011) Simultaneous determination of quality parameters of biodiesel/diesel blends using HATR-FTIR spectra and PLS, iPLS or siPLS regressions. Fuel 90:701–706. doi: 10.1016/j.fuel.2010.09.016
46. Mitroka SM, Smiley TD, Tanko JM, Dietrich AM (2013) Reaction mechanism for oxidation and degradation of high density polyethylene in chlorinated water. Polym Degrad Stab 98:1369–1377. doi: 10.1016/j.polymdegradstab.2013.03.020
47. De Paoli M-A (2008) Degradação e Estabilização de Polímeros, 2nd ed. Chemkeys
48. Pontes IF, Almeida SLM de (2005) Talco.
49. Hahladakis JN, Velis CA, Weber R, et al (2018) An overview of chemical additives present in plastics: Migration, release, fate and environmental impact during their use, disposal and recycling. J Hazard Mater 344:179–199. doi: 10.1016/j.jhazmat.2017.10.014
50. Coutinho FMB, Mello IL, Santa Maria LC de (2003) Polietileno: principais tipos, propriedades e aplicações. Polímeros 13:1–13. doi: 10.1590/S0104-14282003000100005

51. Pereira KR de O (2008) Estudo, em escala de laboratório, do uso de argilas do tipo Bofe na obtenção de argilas organofílicas e ativadas. Universidade de São Paulo
52. Alves RB (2008) Desenvolvimento de nanocompósito de polietileno de baixa densidade pós-consumo reciclado/bentonita. Universidade Federal de Pernambuco
53. Zare Y (2013) Recent progress on preparation and properties of nanocomposites from recycled polymers: A review. Waste Manag 33:598–604. doi: 10.1016/j.wasman.2012.07.031
54. de Paiva LB, Morales AR, Valenzuela Díaz FR (2008) Organoclays: Properties, preparation and applications. Appl Clay Sci 42:8–24. doi: 10.1016/j.clay.2008.02.006
55. Caro E, Comas E (2017) Polyethylene comonomer characterization by using FTIR and a multivariate classification technique. Talanta 163:48–53. doi: 10.1016/j.talanta.2016.10.082
56. Gulmine J V., Janissek PR, Heise HM, Akcelrud L (2002) Polyethylene characterization by FTIR. Polym Test 21:557–563. doi: 10.1016/S0142-9418(01)00124-6
57. Luijsterburg B, Goossens H (2014) Assessment of plastic packaging waste: Material origin, methods, properties. Resour Conserv Recycl 85:88–97. doi: 10.1016/j.resconrec.2013.10.010
58. Babaghayou MI, Mourad A-HI, Lorenzo V, et al (2016) Photodegradation characterization and heterogeneity evaluation of the exposed and unexposed faces of stabilized and unstabilized LDPE films. Mater Des 111:279–290. doi: 10.1016/j.matdes.2016.08.065
59. Martínez-Romo A, González-Mota R, Soto-Bernal JJ, Rosales-Candelas I (2015) Investigating the Degradability of HDPE, LDPE, PE-BIO, and PE-OXO Films under UV-B Radiation. J Spectrosc 2015:1–6. doi: 10.1155/2015/586514
60. Signoret C, Caro-Bretelle A-S, Lopez-Cuesta J-M, et al (2019) MIR spectral characterization of plastic to enable discrimination in an industrial recycling context: II. Specific case of polyolefins. Waste Manag 98:160–172. doi: 10.1016/j.wasman.2019.08.010
61. Fang J, Zhang L, Sutton D, et al (2012) Needleless Melt-Electrospinning of Polypropylene Nanofibres. J Nanomater 2012:1–9. doi: 10.1155/2012/382639
62. El-Saftawy AA, Elfalaky A, Ragheb MS, Zakhary SG (2014) Electron beam induced surface modifications of PET film. Radiat Phys Chem 102:96–102. doi: 10.1016/j.radphyschem.2014.04.025
63. Pereira AP dos S, Silva MHP da, Lima Júnior ÉP, et al (2017) Processing and Characterization of PET Composites Reinforced With Geopolymer Concrete Waste. Mater Res 20:411–420. doi: 10.1590/1980-5373-mr-2017-0734
64. Edge M, Wiles R, Allen NS, et al (1996) Characterisation of the species responsible for yellowing in melt degraded aromatic polyesters—I: Yellowing of poly(ethylene terephthalate). Polym Degrad Stab 53:141–151. doi: 10.1016/0141-3910(96)00081-X
65. Salgado BCB, Valentini A (2019) EVALUATION OF THE PHOTOCATALYTIC ACTIVITY OF SiO2@TiO2 HYBRID SPHERES IN THE DEGRADATION OF METHYLENE BLUE AND HYDROXYLATION OF BENZENE: KINETIC AND MECHANISTIC STUDY. Brazilian J Chem Eng 36:1501–1518. doi: 10.1590/0104-6632.20190364s20190139

66. Rodriguez-Blanco JD, Shaw S, Benning LG (2011) The kinetics and mechanisms of amorphous calcium carbonate (ACC) crystallization to calcite, viavaterite. Nanoscale 3:265–271. doi: 10.1039/C0NR00589D
67. Maleki Dizaj S, Barzegar-Jalali M, Zarrintan MH, et al (2015) Calcium carbonate nanoparticles as cancer drug delivery system. Expert Opin Drug Deliv 12:1649–1660. doi: 10.1517/17425247.2015.1049530
68. Xu B, Poduska KM (2014) Linking crystal structure with temperature-sensitive vibrational modes in calcium carbonate minerals. Phys Chem Chem Phys 16:17634–17639. doi: 10.1039/C4CP01772B
69. Netzloff HM, Collins MA (2007) Ab initio energies of nonconducting crystals by systematic fragmentation. J Chem Phys 127:134113. doi: 10.1063/1.2768534
70. Zhang M, Li J, Zhao J, et al (2020) Comparison of CH 4 and CO2 Adsorptions onto Calcite(10.4), Aragonite(011)Ca, and Vaterite(010)CO3 Surfaces: An MD and DFT Investigation. ACS Omega 5:11369–11377. doi: 10.1021/acsomega.0c00345
71. Mohsin MA, Abdulrehman T, Haik Y (2017) Reactive Extrusion of Polyethylene Terephthalate Waste and Investigation of Its Thermal and Mechanical Properties after Treatment. Int J Chem Eng 2017:1–10. doi: 10.1155/2017/5361251
72. Dimonie D, Socoteanu R, Pop S, et al (2012) Overview on Mechanical Recycling by Chain Extension of POSTC-PET Bottles. In: Mater. Recycl. - Trends Perspect. InTech, pp 85–114
73. Miller JN, Miller JC (2010) Statistics and Chemometrics for Analytical Chemistry, 6th ed. Pearson Education, Harlow
74. Van Puyvelde P, Vananroye A, Cardinaels R, Moldenaers P (2008) Review on morphology development of immiscible blends in confined shear flow. Polymer (Guildf) 49:5363–5372. doi: 10.1016/j.polymer.2008.08.055
75. Utracki LA, Wilkie CA (2014) Polymer Blends Handbook, 2nd ed. doi: 10.1007/978-94-007-6064-6
76. Ilyin SO, Makarova V V., Polyakova MY, Kulichikhin VG (2020) Phase behavior and rheology of miscible and immiscible blends of linear and hyperbranched siloxane macromolecules. Mater Today Commun 22:100833. doi: 10.1016/j.mtcomm.2019.100833
77. Liu C, Wang J, He J (2002) Rheological and thermal properties of m-LLDPE blends with m-HDPE and LDPE. Polymer (Guildf) 43:3811–3818. doi: 10.1016/S0032-3861(02)00201-X
78. Banerjee S, Yang R, Courchene CE, Conners TE (2009) Scanning Electron Microscopy Measurements of the Surface Roughness of Paper. Ind Eng Chem Res 48:4322–4325. doi: 10.1021/ie900029v
79. Achilias DS (2012) Material Recycling - Trends and Perspectives. doi: 10.5772/2003
80. Ashton EG, Kindlein W, Demori R, et al (2015) Recycling polymeric multi-material products through micronization. J Clean Prod 116:268–278. doi: 10.1016/j.jclepro.2016.01.018
81. Coltro L, Duarte LC (2013) Reciclagem de embalagens plásticas flexíveis: contribuição da identificação correta. Polímeros 23:128–134. doi: 10.1590/S0104-14282013005000008

Figures

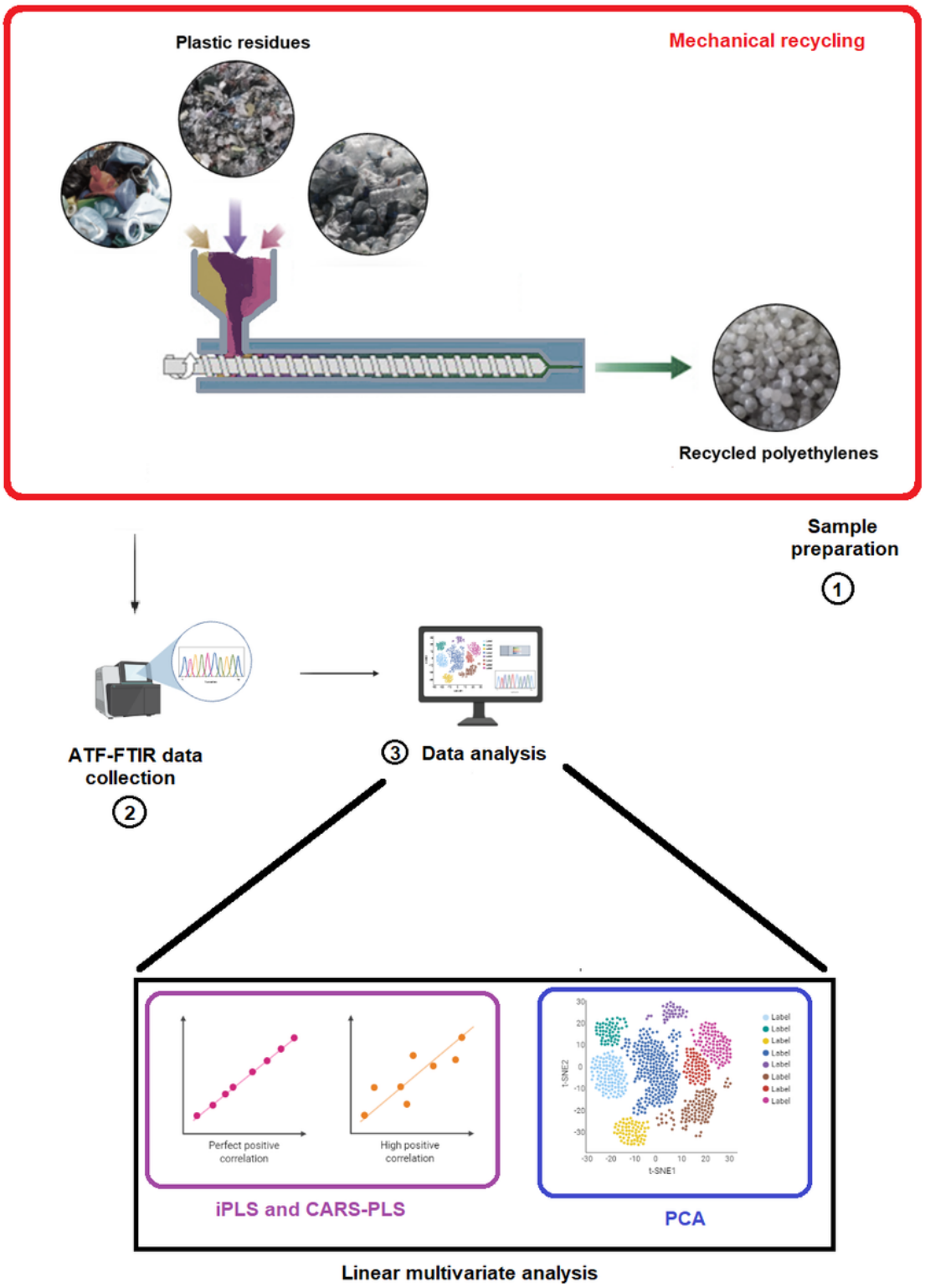

Figure 1

Schematic representation of the experimental procedure.

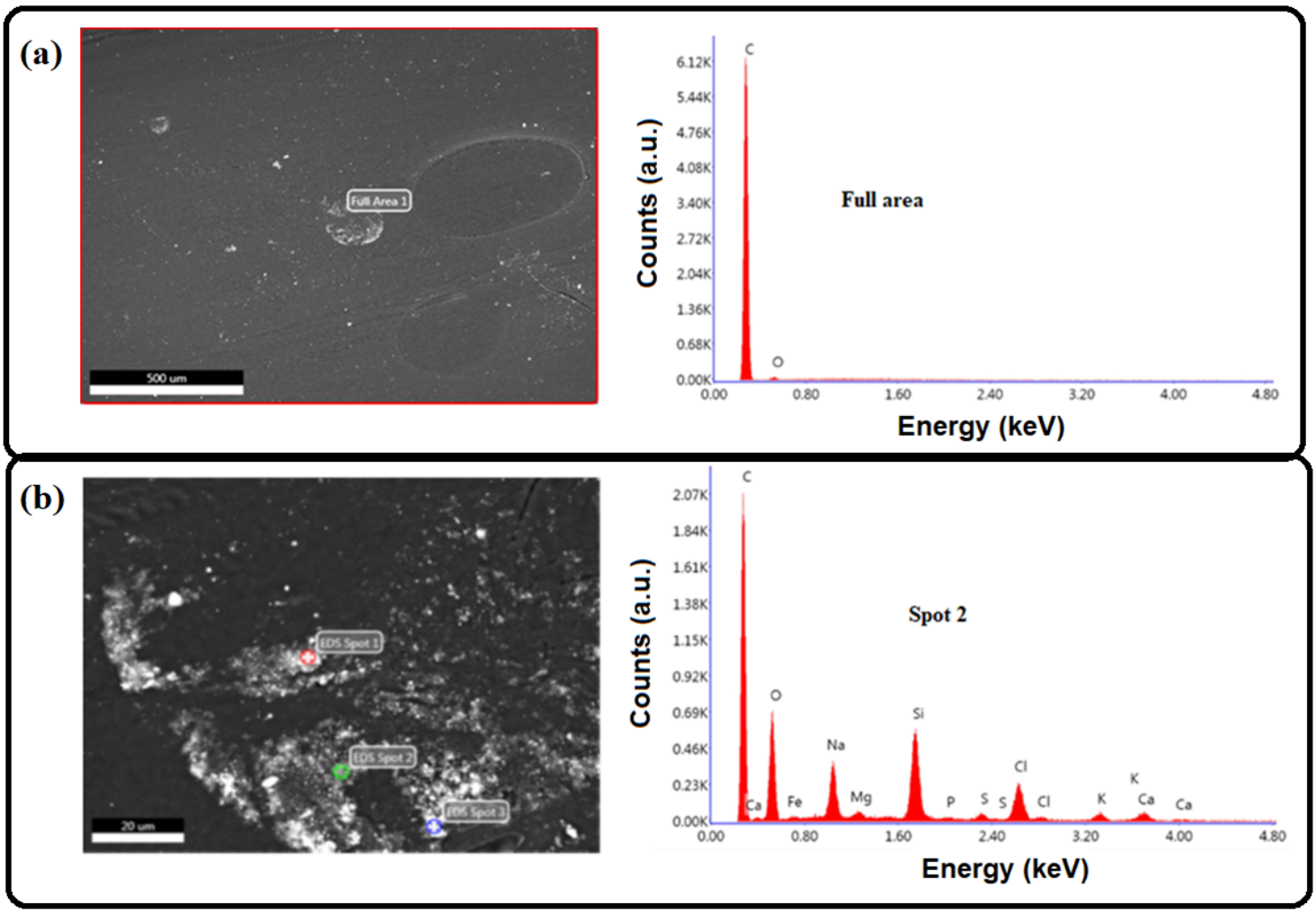

Figure 2

SEMimages (left) and EDS spectra (right) of recycled HDPE. Scale bar of 500μm (a) and 20μm (b).

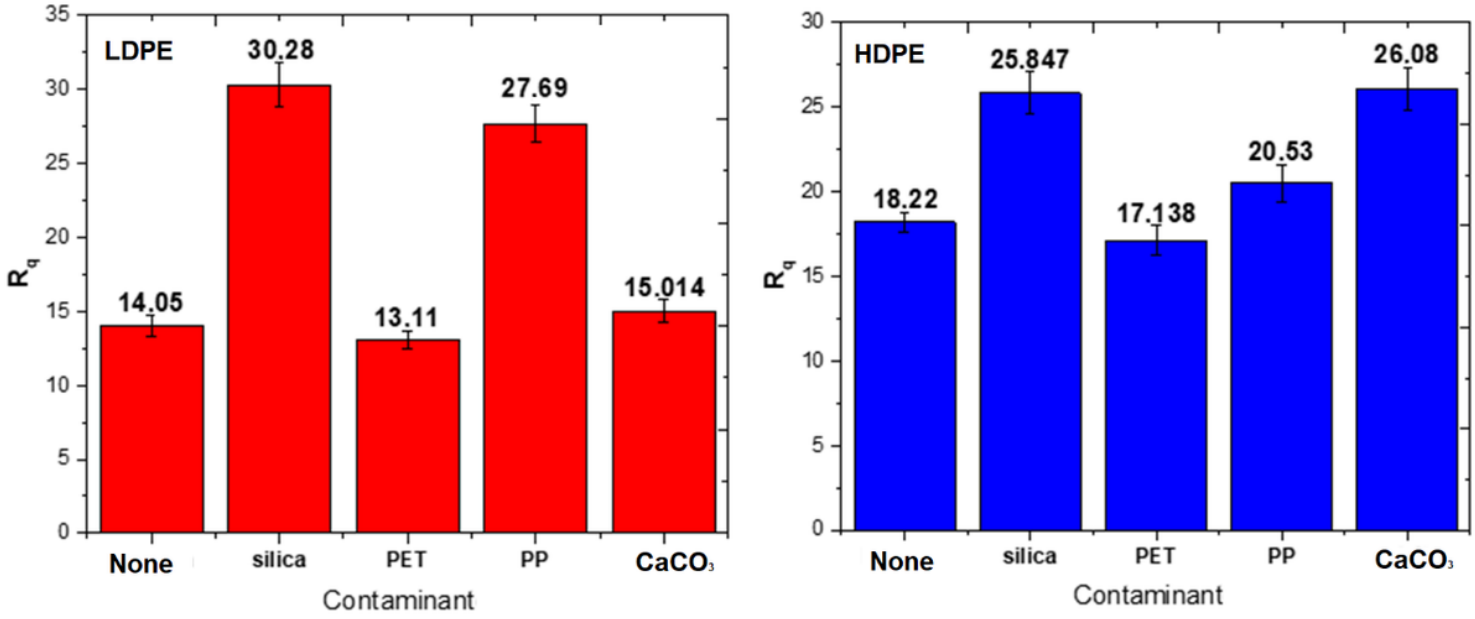

Figure 3

SEM images (left) and EDS spectra (right) of recycled LDPE. Scale bar of 500μm (a) and 20μm (b).

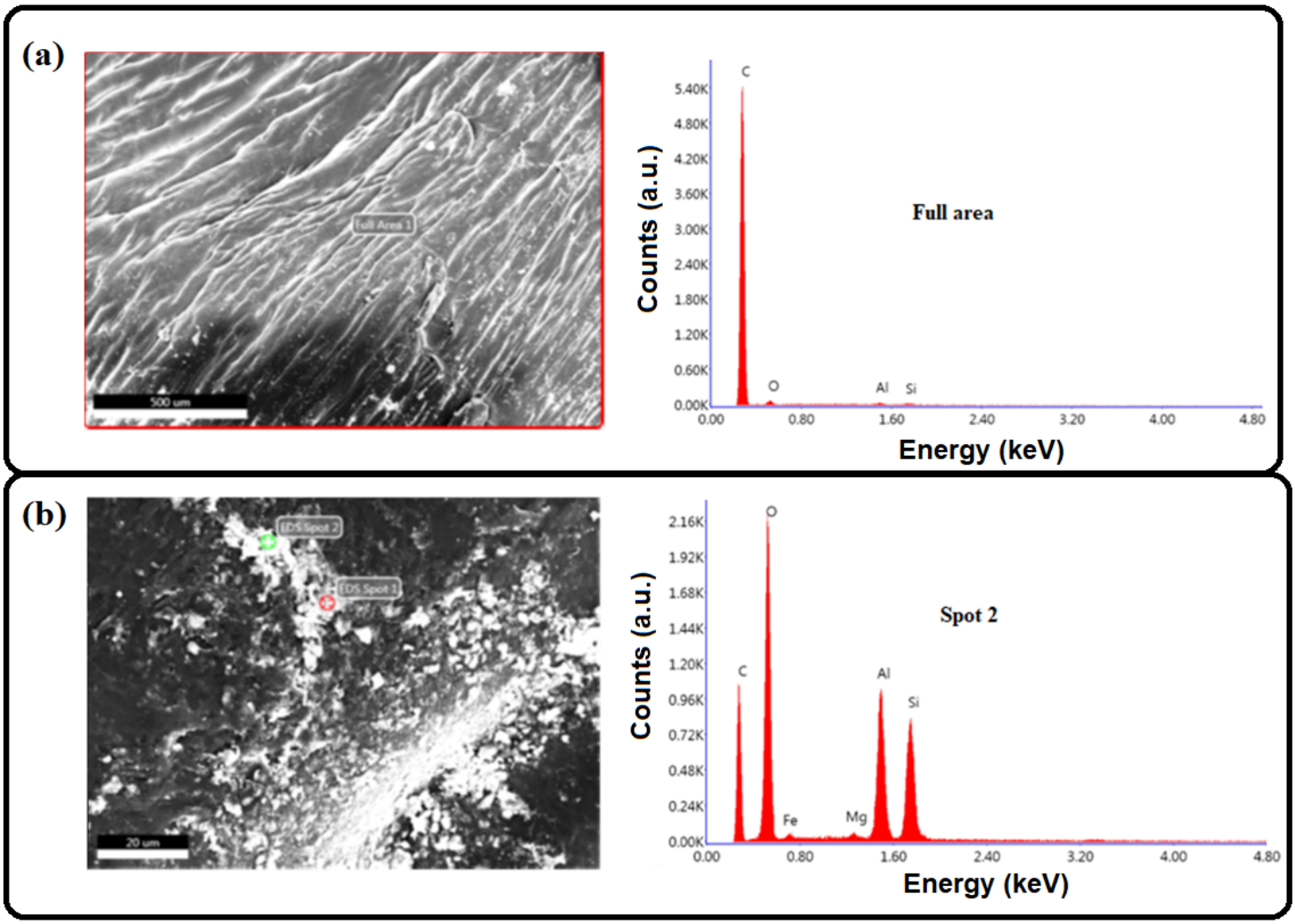

Figure 4

ATR-FTIR absorption bands of LDPE and HDPE (pristine and recycled).

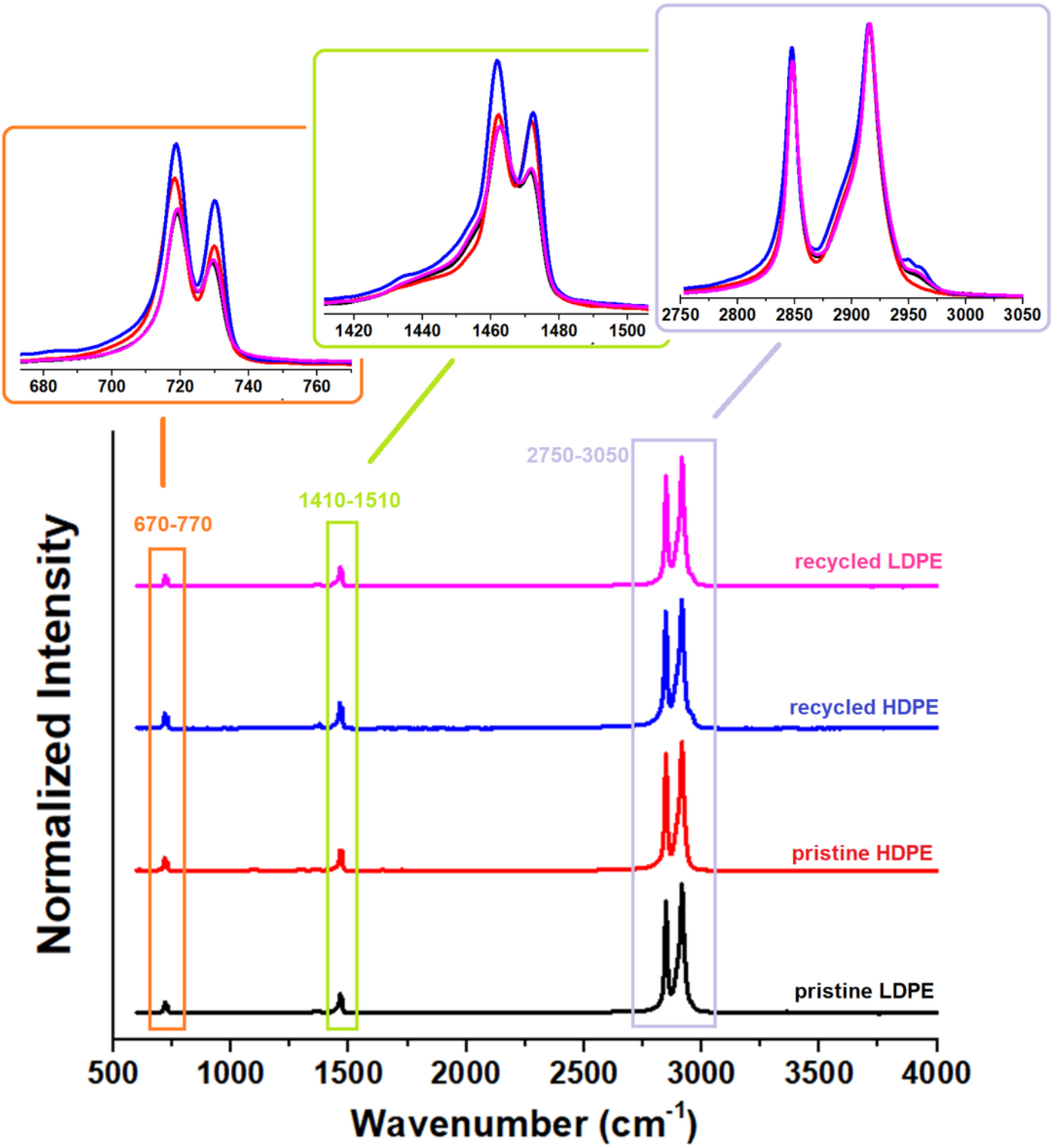

Figure 5

ATR-FTIR absorption bands of recycled PET, recycled PP, silicon dioxide, and calcium carbonate.

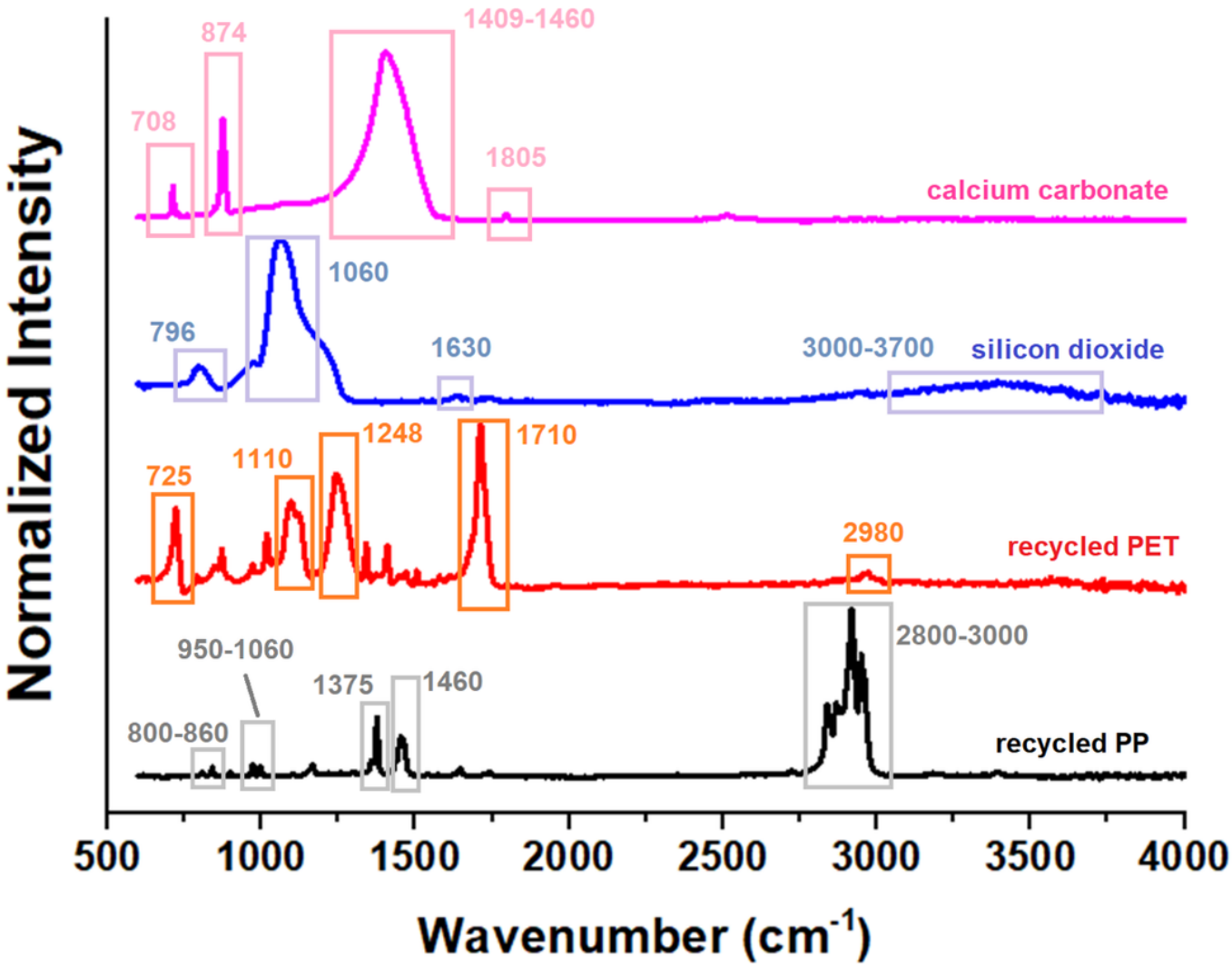

Figure 6

2D (a and c) and 3D (b) diagrams of PC scores from PCA analysis(with 95 % confidence ellipses) for recycled HDPE (rHDPE), recycled (LDPE), pristine HDPE (pHDPE), pristine LDPE (pLDPE), and polyethylene recyclates with 5 wt% of the different known contaminants (silica, calcium carbonate, recycled PP, and recycled PET).

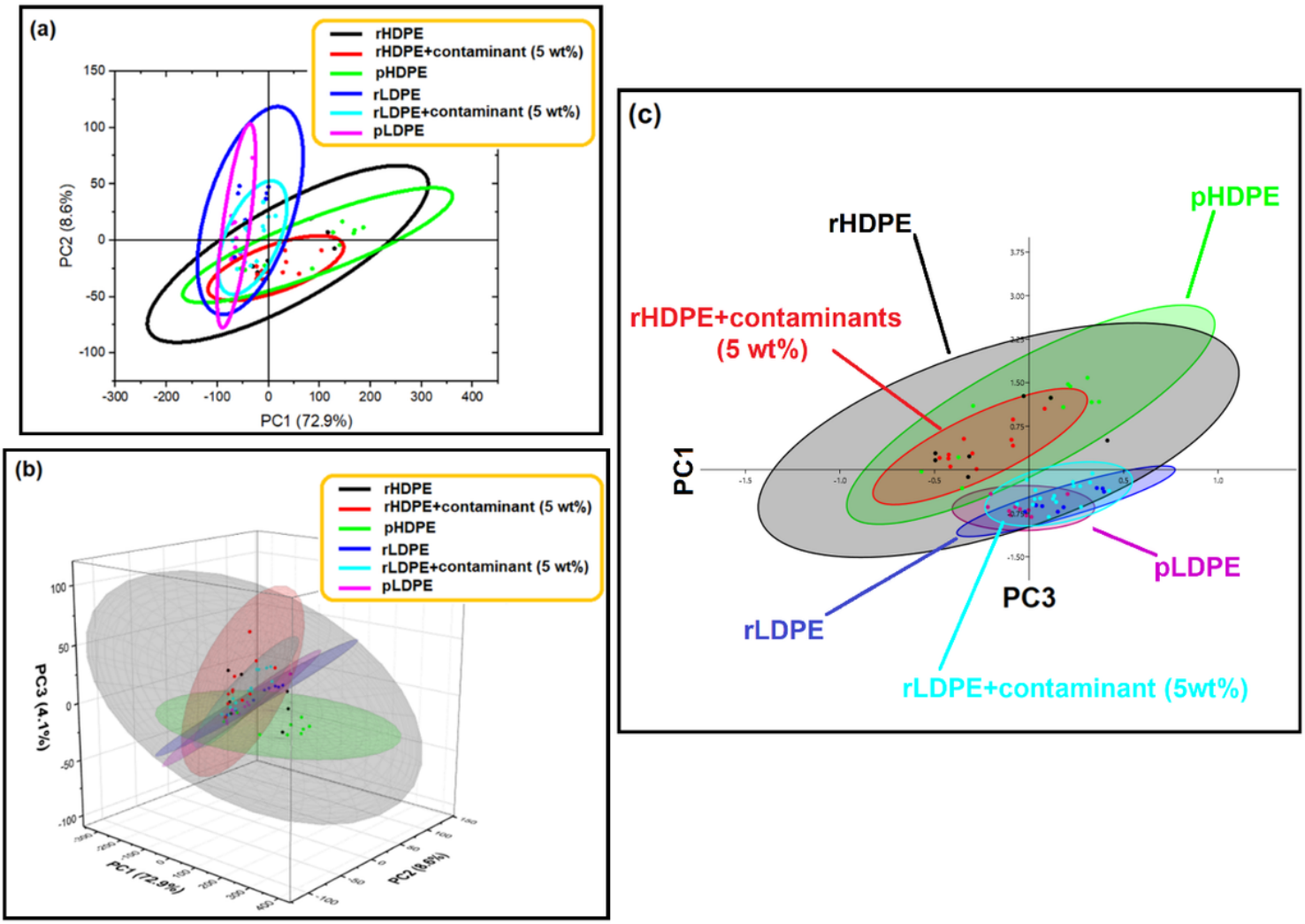

Figure 7

2D (a) and 3D (b) diagrams of PC scores from PCA analysis (with 95 % confidence ellipses) of recycled HDPE/LDPE blends with 5 wt% of the different known contaminants (silicate, calcium carbonate, recycled PP, and recycled PET).

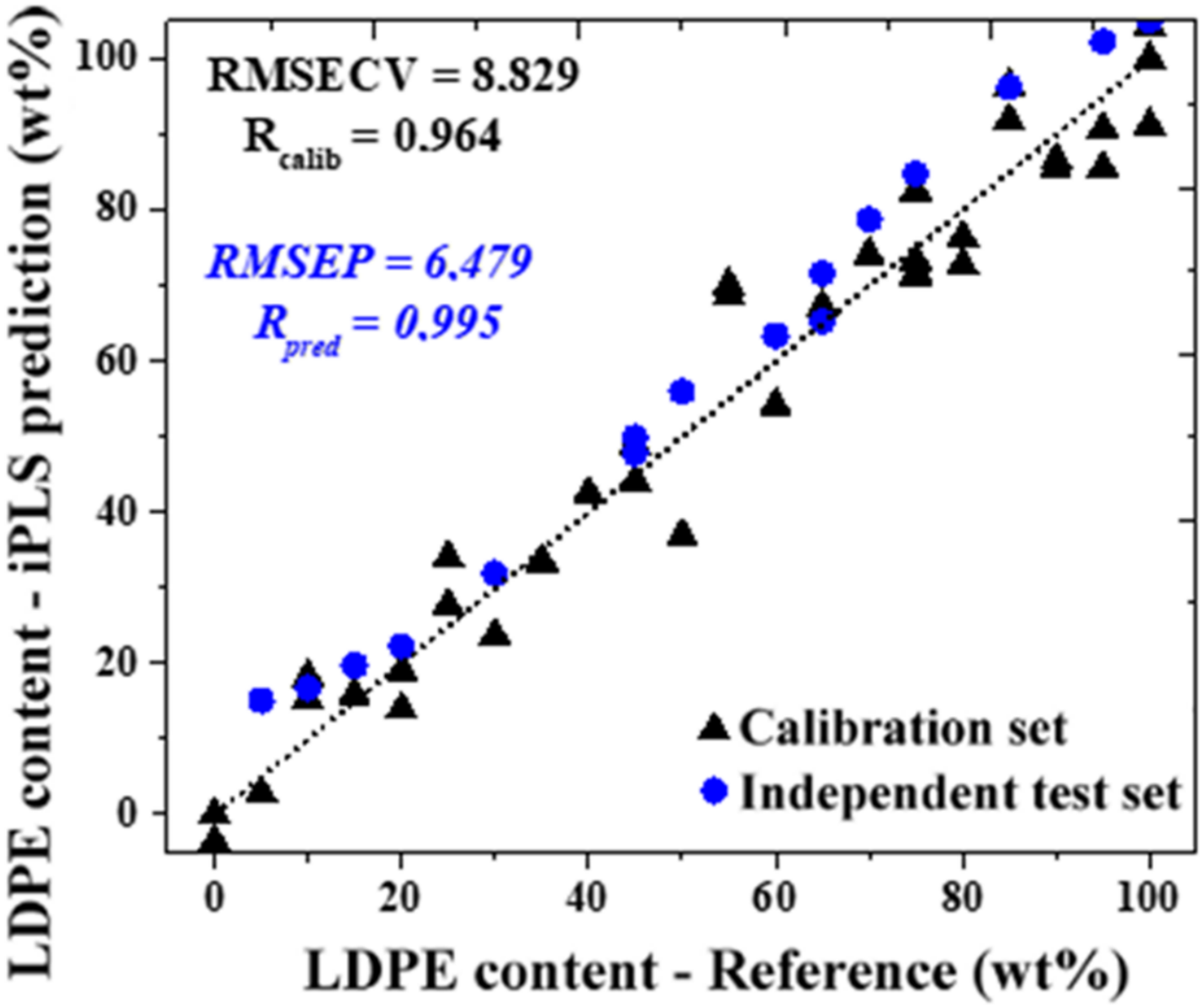

Figure 8

2D diagrams of PC scores from PCA analysis (with 95 % confidence ellipses) of samples based on the plastics: LDPE (a), HDPE (b), and HDPE/LDPE blends (c).

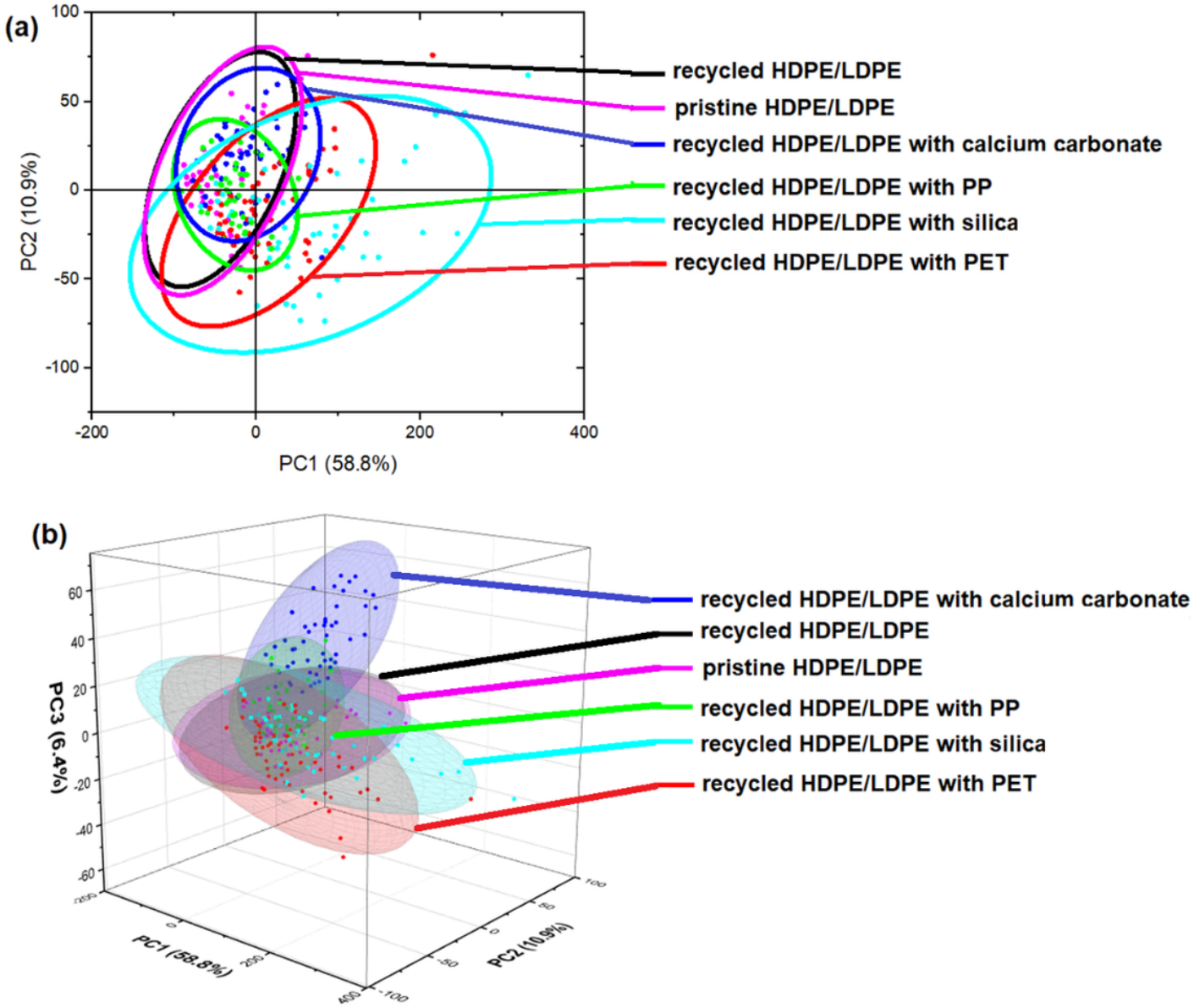

Figure 9

Reference vs. prediction of LDPE content (wt%) in HDPE/LDPE blends (recycled plastics). Data obtained with the CARS/PLS-R model.

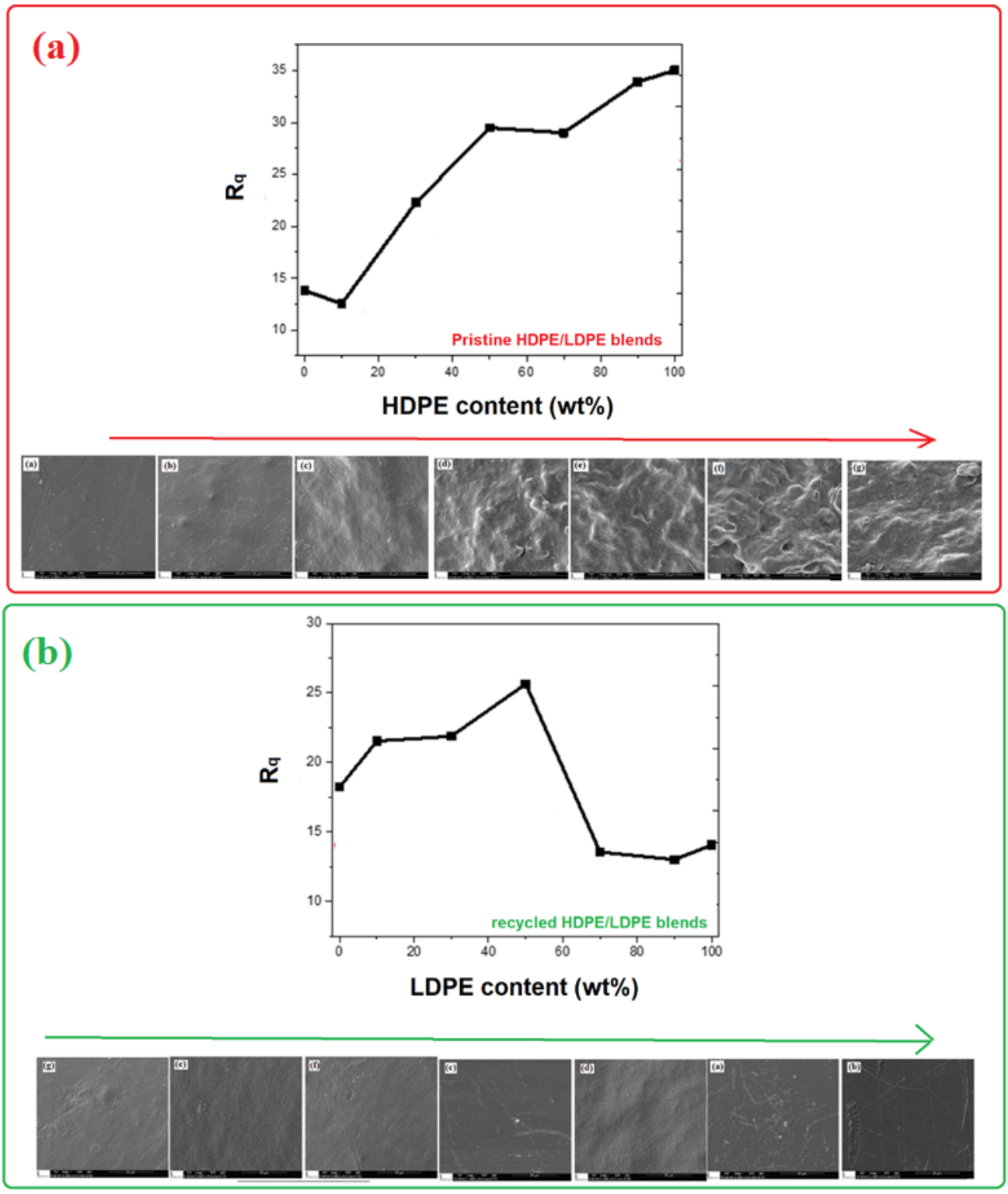

Figure 10

Rq roughness of HDPE/LDPE blends based on pristine (a) and recycled (b) plastics.

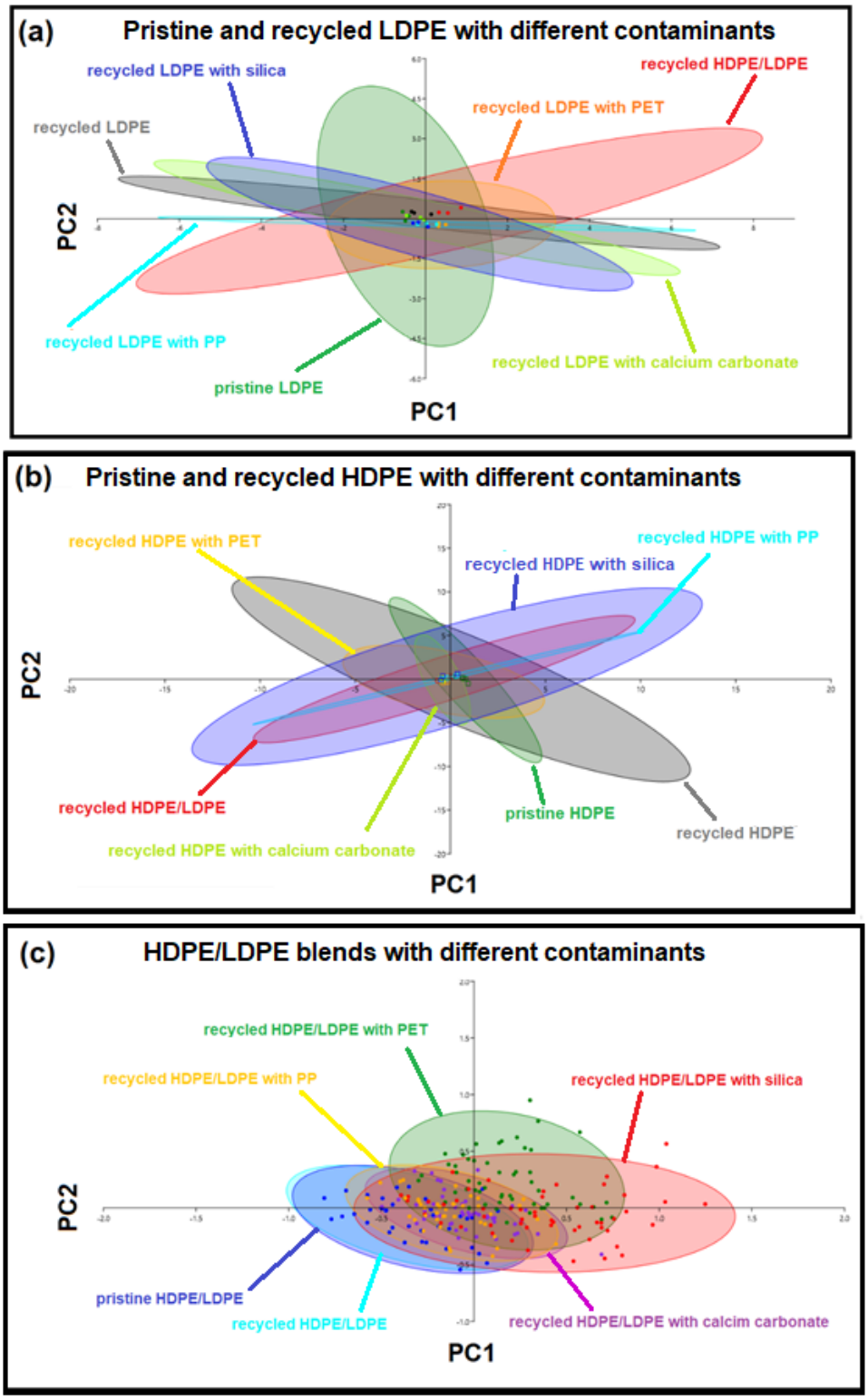

Figure 11

Reference vs. prediction of LDPE content (wt%) in recycled HDPE/LDPE blends using iPLS-R.

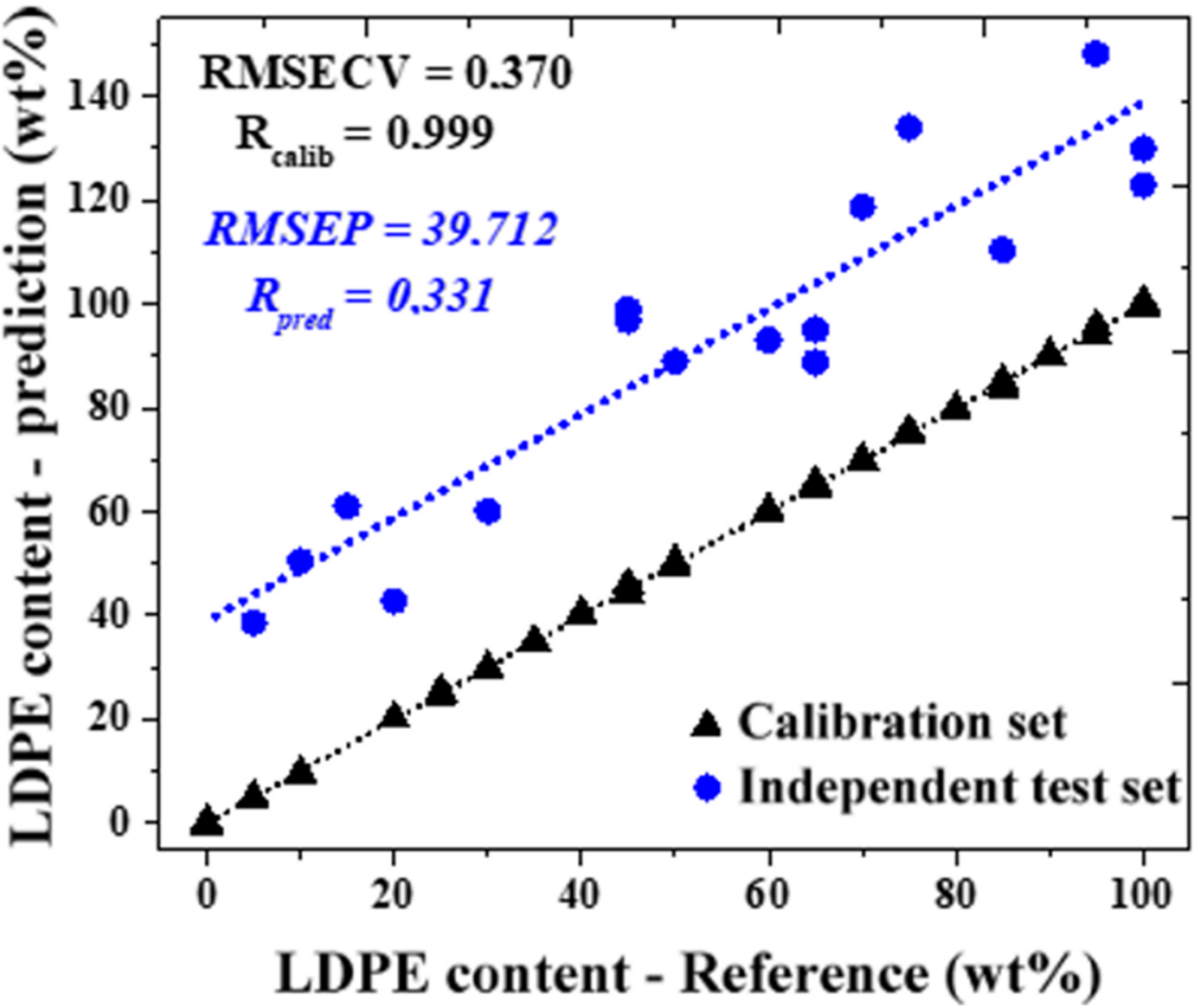

Figure 12

Reference vs. prediction of the LDPE content (wt%) in the recycled HDPE/LDPE blends. Data obtained with the iPLS-R model and ATR-FTIR spectral data. The recycled polymeric blends contain 5wt% of different contaminants: (a) CaCO3, (b) PET, (c) PP, and (d) silica gel.

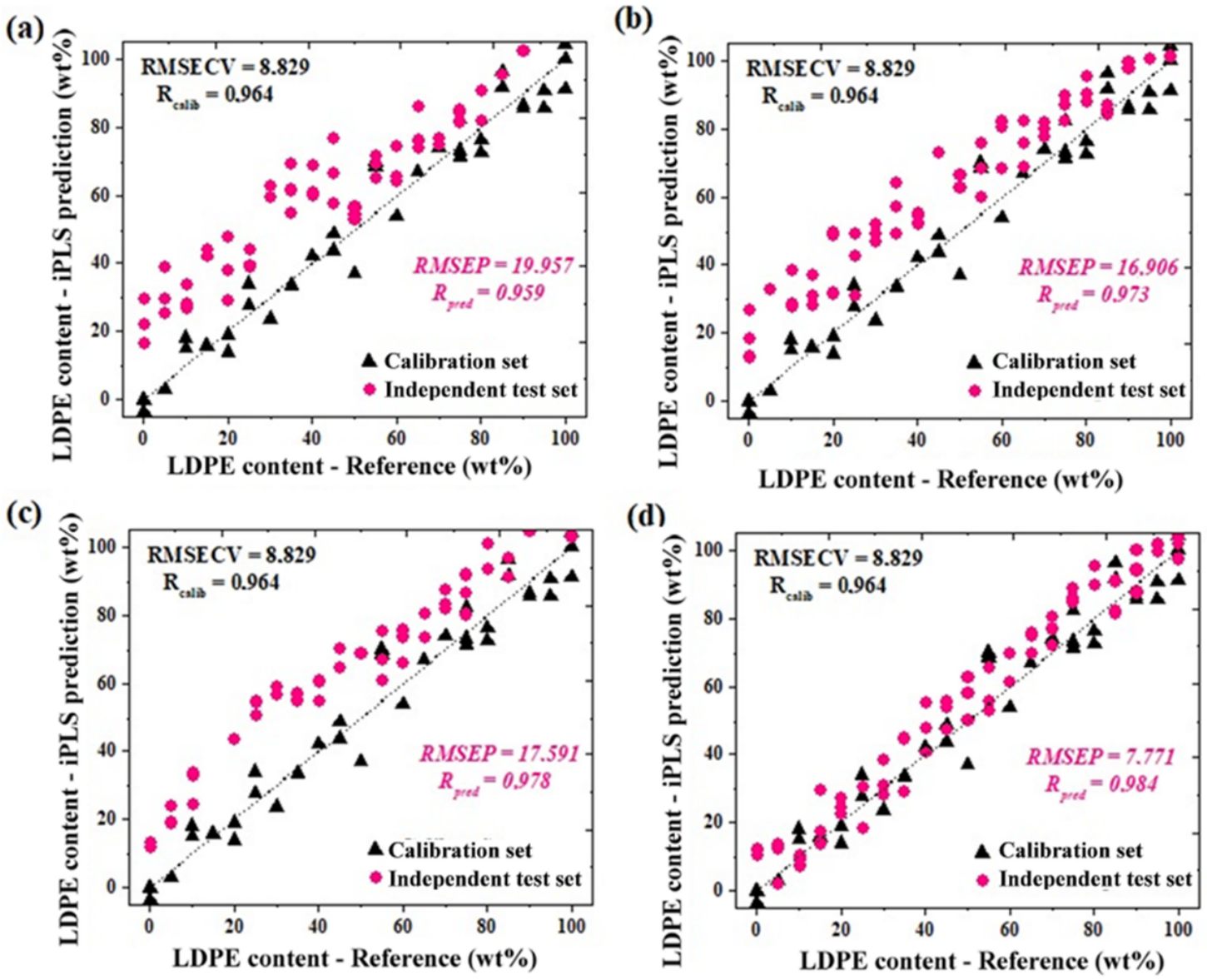

Figure 13

Variation of Rq roughness in recycled HDPE (blue bars) and recycled LDPE (red bars) pellets due to different contaminants.

Supplementary Files

This is a list of supplementary files associated with this preprint. Click to download.

- SupplementaryMaterials.docx